Flexible Grid Connection and Islanding of SPC-Based PV Power Converters

Pedro Rodríguez, *Fellow, IEEE*, Costantino Citro, J. Ignacio Candela, *Member, IEEE*, Joan Rocabert, *Member, IEEE*, and Alvaro Luna, *Member, IEEE*

***Abstract*—At the present time, distributed generation systems are required to disconnect from the main grid when there is an outage. In order to fulfill this requirement, photovoltaic (PV) power plants are equipped with anti-islanding algorithms, embedded in the converters controller, to avoid the island operation. However, the current trends in the development of the future electrical networks evidence that it is technically feasible and economically advantageous to keep feeding islanded systems under these situations, without cutting the power supply to the loads connected to the network. Nevertheless, commercial PV power converters are programmed as grid-feeding converters and they are unable to work in island mode if there is not an agent forming the grid. In order to overcome this problem, the synchronous power controller (SPC) is presented in this paper as a suitable alternative for controlling PV inverters. As will be further discussed, this controller permits PV plants to operate seamlessly in grid-connected and island mode, with no need of changing the control structure in either case. Moreover, the participation of SPC-based power converters integrating energy storage enables other grid-feeding systems to contribute to the grid operation in island conditions. The good results achieved with the SPC in different conditions will be shown in simulations, and also with experiments considering a real PV power plant combining SPC and commercial PV inverters.**

***Index Terms*—DC–AC power converters, distributed power generation, electric variables control, photovoltaic (PV) systems.**

I. Introduction

IN SPITE of the increasing penetration of distributed generation (DG) systems [1]–[2], the intentional island operation is still not permitted for generation systems, which are connected to the main electrical network. Thus, no matter the availability of energy resources, local generation systems are forced to trip when there is an outage in the main grid, with no prejudice of repowering an islanded system after several seconds. However, this operation mode does not prevent the local loads from suffering a total disconnection for some seconds, which, in an industrial environment, is translated into a complete restart of a production process or a reload of information and communication technologies (ICT) systems [3].

Photovoltaic (PV)-based power plants are not an exception among the DG facilities, and they are required to detect the island condition and cease feeding the line with power within a short period of time [4]–[5]. Due to this, the implementation of anti-islanding algorithms is compulsory in all grid-connected PV systems. In this case, the main reason behind this disconnection lies in the fact that a failed disconnection of the power conversion system interfacing a PV plant may result in undesired consequences, such as equipment damages or safety hazard for the grid utility operators.

In order to meet the anti-islanding requirements imposed by the standards, the PV inverter manufacturers include advanced islanding detection algorithms [6]. Among the different solutions, two main categories of islanding detection algorithms are proposed: passive and active methods [7]. In passive methods, the islanding detection relies exclusively on monitoring the grid characteristics at the point of common coupling (PCC), on the grounds that the power mismatch between production and consumption obtained after a grid disconnection determines a clear change in one of the main system parameters, such as voltage amplitude, frequency, phase jumps, or harmonic distortion [8]–[9].

On the other hand, active methods are based on influencing the state of the grid by generating intentionally currents or voltages distortions, in such a way that the grid presence/absence can be inferred based on the obtained response [10]–[11]. Some of the active methods proposed in the literature are based on the estimation of the grid impedance, on the grounds that a significant variation of this value is produced after a disconnection of the main grid. However, the effectiveness of this method decreases if multiple inverters are connected in parallel or if there is a significant harmonic component in the line current. Other active methods are based on forcing a deviation, either in the frequency or in the voltage amplitude. As long as the grid is present, the voltage waveform at the PCC will not change, but, when there is no grid, these parameters will change until the anti-islanding algorithm trips the out-of-range protections [12].

This work was supported by the Spanish Ministry of Economy and Competitive-ness under Project ENE2014-60228-R. *(Corresponding author: Alvaro Luna.)*

P. Rodríguez is with the Department of Electrical Engineering, Technical University of Catalonia, Barcelona 08222, Spain, and also with the University of Loyola Andalucia, Seville 41014, Spain (e-mail: prodriguez@ee.upc.edu).

C. Citro is with the University of Salerno, Fisciano 84084, Italy (e-mail: costantino.citro@upc.edu).

J. I. Candela, J. Rocabert, and A. Luna are with the Department of Electrical Engineering, Technical University of Catalonia, Barcelona 08222, Spain (e-mail: candela@ee.upc.edu; rocabert@ee.upc.edu; luna@ee.upc.edu).

However, the capability of DG systems of feeding microgrids with intentional islanding capability and the development of advanced grid control systems allays the anti-islanding requirements. Nevertheless, at the present time, PV power converters work in grid-feeding mode in the vast majority of applications, based on following a current reference. As stated in [13], grid-feeding converters cannot work properly if there is no network forming the voltage. Therefore, the anti-islanding standards are not the only issue to overcome, but it is necessary to find new control methodologies for PV systems in order to enable them to operate either in grid-connected or islanded mode without affecting the operation of the network and the plant itself.

Some studies have been published about microgrids operation during disconnection and reconnection transitions in front of any outage of the main grid, minimizing disturbances, and undesired transients [14]–[15]. The operation of the microgrid in steady state is defined by the good performance of the controllers implemented at the DG systems, as well as by the linear and nonlinear load-sharing functionalities [16]. However, all these solutions require complex control algorithms dedicated exclusively to solve grid forming situations in the event of island operation and detection.

In this regard, the SPC, which was presented in [17]–[18] and licensed under the patents [19], [20], and [21], constitutes a good alternative for controlling islanded microgrids, energy storage (ES) devices and PV power converters under all kind of conditions. As detailed in [18], the SPC permits to control PV power converters and ES devices, no matter if they are grid-connected, driven by an maximum point power tracking (MPPT) algorithm, or in island mode, as it is able also to work as a grid-forming system, without changing the inner control layer of the converter. It is just necessary to consider that, in a PV application, the power is unidirectional and, hence, no more power than the one delivered by the panels can be handled.

In this paper, the application of the SPC in PV converters and ES devices and their suitable performance when operating in networks, which can be either seamlessly connected or disconnected from the main grid without affecting the power supply to the loads, are analyzed. Moreover, in order to demonstrate the compatibility of the proposed controller, the SPC-based converter has been connected in parallel with other commercial PV grid-feeding converters and loads. As will be shown, through simulations and experiments, the integration of SPC in PV converters and ES devices enables the creation of islanded networks involving other generation systems and jump from grid-connected to island without affecting their operation.

II. Synchronous Power Controller

As described in [22]–[25], it is possible to control a grid-connected generation system, governed by a power converter, in order to reproduce the same performance and dynamic behavior of a classical synchronous generation system. However, different solutions based on the implementation of the synchronous machine model in the control algorithm have been proposed. In [23] and [24], the behavior of synchronous generator is mimicked in the control of the converter through the machine swing equations with a virtual impedance. This concept is implemented to synchronize the dc–ac converter before connecting to the grids; however, once the system is synchronized with the grid, the virtual impedance loop is disconnected and the converter acts as a voltage-controlled inverter. In [25], the machine swing equations with the virtual admittance concept are permanently applied in the control loop to generate the current reference. This current reference is compared with the current measure in the current control loop to generate the duties to be sent to the power module. This is advantageous, as synchronous generation does not require a complex grid synchronization; it provides simplicity in the parallelization of generation units, has an inherent grid-supporting capability and a harmonious operation with the rest of the electrical system.

However, taking advantage of the fact that a power converter is a fully controllable device, it is not only possible to emulate the operation of a synchronous generation system, but even to improve it through online modifications of the characteristics parameters of the virtual machine [25]. In this regard, the SPC constitutes a new and effective solution to integrate power generators driven by power converters, based on power electronics, into the electrical network, gathering the main advantages of synchronous generators operation while overcoming the main drawbacks.

A. Electrical Control Loop

The electrical interaction in the connection of a conventional synchronous generator can be described by the following differential equation:

$$v\left(t\right) = e\left(t\right) - R \cdot i\left(t\right) - L \cdot \frac{di\left(t\right)}{dt} \tag{1}$$

where v is the ac voltage at the point of connection, e is the induced electromotive force, i is the current, and finally, RL represents the output impedance of the generator.

This equation can be implemented in the control layer of a power converter, in order to mimic the electrical performance of the synchronous generator. In such case, the impedance is not physically connected at the output of the converter, but it is virtually implemented in the digital controller of the converter. This approach has been extensively used and its performance has been reported in [26]–[28]. However, the virtual impedance structure presents some issues.

The main one lies in the fact that the virtual impedance concept presents serious control problems when the measured current is affected by harmonics, transients, or even noise in the measurements.

As reported in [18], the SPC overcomes this issue by implementing an electrical characteristic based on using a virtual admittance, $Y(s)$. In such a way, the power converter is controlled as a current source and there is no derivative terms affecting the controller, as can be seen in the next expression, written in the Laplace domain

$$i = Y \cdot (e - v) \quad ; \quad Y(s) = \frac{1}{R + sL}. \tag{2}$$

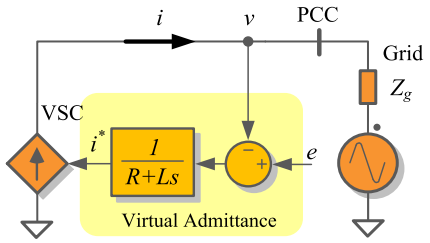

Fig. 1. Electrical control loop based on a virtual admittance.

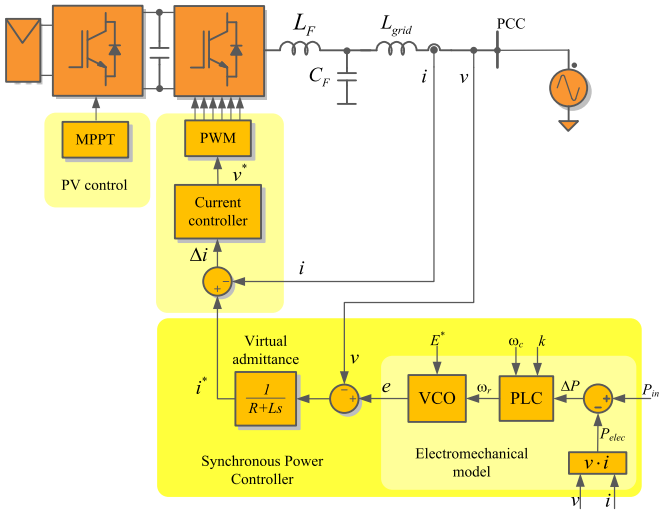

Fig. 2. Electromechanical control loop of the SPC.

A simplified layout of the proposed controller is depicted in Fig. 1, where the power converter is presented as current source.

As introduced in [17] and [18], this performance is achieved in a real application, including an inner current control loop, as shown in the layout depicted in Fig. 1, for a PV power converter case.

B. Electromechanical Control Loop

In the SPC controller, the electrical control loop gets the reference of the internal electromotive force e from the output of the electromechanical model, as shown in Fig. 2.

As introduced in [17] and [18], the power between the power delivered and absorbed by the converter, ΔP, in a synchronous generator is the one that gives rise to the acceleration and deceleration of the mechanical part, thus changing the mechanical speed ω_{r} following the dynamic response of a rotational system. The change in the speed is translated into a variation of the electromotive force in the generator.

Therefore, as stated in [29] and [30], the electromechanical model can implement the same function that is obtained from a real synchronous generator, which involves mainly the inertia of the machine, giving rise to an overall transfer function between the mechanical power (input) and the electrical power (output) in a synchronous generator with very low damping, which is

$$\frac{P_{\mathrm{elec}}}{P_{\mathrm{mec}}} = \frac{\omega_n^2}{s^2+\omega_n^2} = \frac{\frac{P_{\mathrm{Max}}}{J\cdot\omega_s}}{s^2+\frac{P_{\mathrm{Max}}}{J\cdot\omega_s}} \tag{3}$$

where ω_s is synchronous angular speed, J is the inertia of the generator, and P_{Max}, which is the theoretical maximum power that an equivalent generator would be able to deliver without hindering the stability.

However, due to the fact that this layer is also fully programmable, an advanced electromechanical characteristic, with controllable damping factor and adjustable inertia, can be programmed. This solution is adopted in the SPC, giving rise to an overall dynamic of the SPC that responds to the following transfer function:

$$\frac{P_{\mathrm{elec}}}{P_{\mathrm{mec}}} = \frac{\omega_n^2}{s^2+2\xi\omega_n s+\omega_n^2} \tag{4}$$

where ξ is the damping factor and ω_n is the natural frequency of the SPC. As introduced in [17] and [18], this response can be achieved if a power loop controller block is introduced; in this case, the following transfer function is proposed:

$$\mathrm{PLC}(s) = k\frac{\omega_c}{s+\omega_c} \tag{5}$$

where the gain k and the cutoff frequency ω_c of the controller can be calculated as a function of the natural frequency ω_n and the damping factor ξ of the closed-loop function is as follows:

$$\begin{aligned} \omega_c &= \frac{\omega_n}{2\xi P_{\mathrm{max}}} \\ k &= 2\xi\omega_n \end{aligned} \tag{6}$$

giving rise to the following virtual inertia in the SPC controller:

$$J = \frac{P_{\mathrm{max}}}{\omega_n^2\omega_s} \quad \left[\mathrm{kg\,m^2}\right]. \tag{7}$$

Considering these demands, this paper will consider that the estimation of the voltage conditions will be carried out within 20–25 ms, as this target permits it to fulfill the most restrictive requirements, in terms of dynamical response, available in the grid codes. This condition will be extended to frequency estimation, although this parameter is more related to secondary control algorithms than low voltage ride through (LVRT), the same time window between 20 and 25 ms will be considered in this paper for the detection of the disturbance.

III. Control in Grid-Connected Conditions

One of the main advantages of the SPC lies in the fact that it can be implemented in any existing power converter, provided that its current control loop is fast and accurate, in order to track the current reference provided by the SPC. The SPC, implemented in a customized system, as the design of the current controller, based on a proportional-resonant (PR) controller, will be detailed [31].

Considering that the system under control is the one depicted in Fig. 2, the following simplified block diagram can be used for showing the inner control loop structure.

In the current control scheme, as shown in Fig. 3, a stationary reference frame is adopted to implement the control, and a PR is adopted as the current controller. The modulation and acquisition delay is considered in the current control loop in order to conduct an accurate modeling and tuning. The expression of

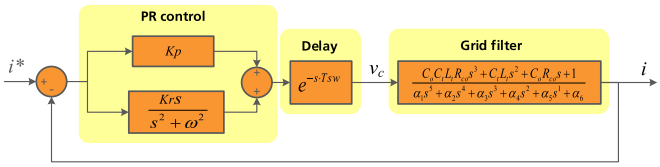

Fig. 3. Structure of the current controller implemented in the inner layer of the SPC controller.

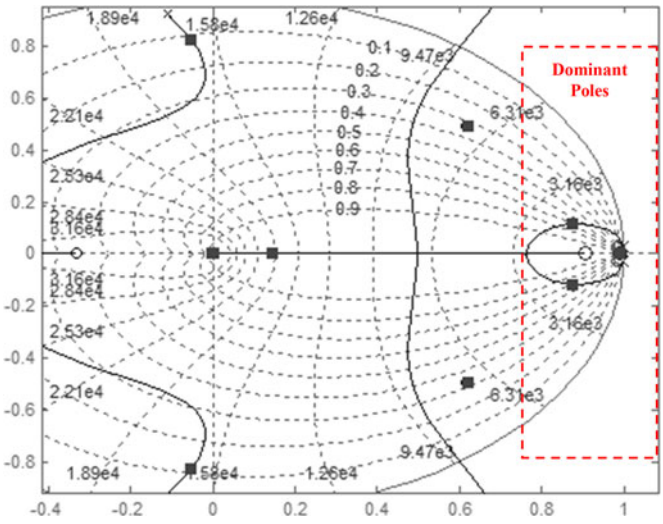

Fig. 4. Root locus diagram of the current controller closed-loop system.

TABLE I
TUNING OF THE PR CONTROLLER IN 10 KW SETUP

Symbol	Quantity	Value
K_p	Proportional gain	6.5
K_r	Resonant gain	18.2
P_{hm}	Phase Margin	50°
G_m	Gain Margin	10.3 dB
ω	nominal ac frequency	314.16 rad/s
ω_b	Bandwidth	$4.7{\cdot}10^3$ rad/ s
t_{ss}	Settling time	11.7 ms

this delay is not exclusive and is determined by the switching frequency and the implementation strategy of the modulation. The LCL filter is the most extended grid connection filter, in this case an LCL plus a trap filter for the switching frequency has been selected, giving rise to a fifth-order system.

Considering the study case of a 10 kVA grid connected power converter with $LCL+$ trap filter, which is the one used in the experimental platform, a *Phm* between (45° and 70°) is specified to avoid any undesired oscillations or overshoot during the transient and steady state. Likewise, the Gm is selected to be above 10 dB. The tuning of the controllers and system stability has been performed via root locus analysis, as shown in Fig. 4. The final parameters selected for the experimental setup are shown in Table I.

The root locus method has been selected, as just the open loop transfer function of the direct chain gives rise to a seventh-order transfer function, as minimum. In these kinds of systems, the

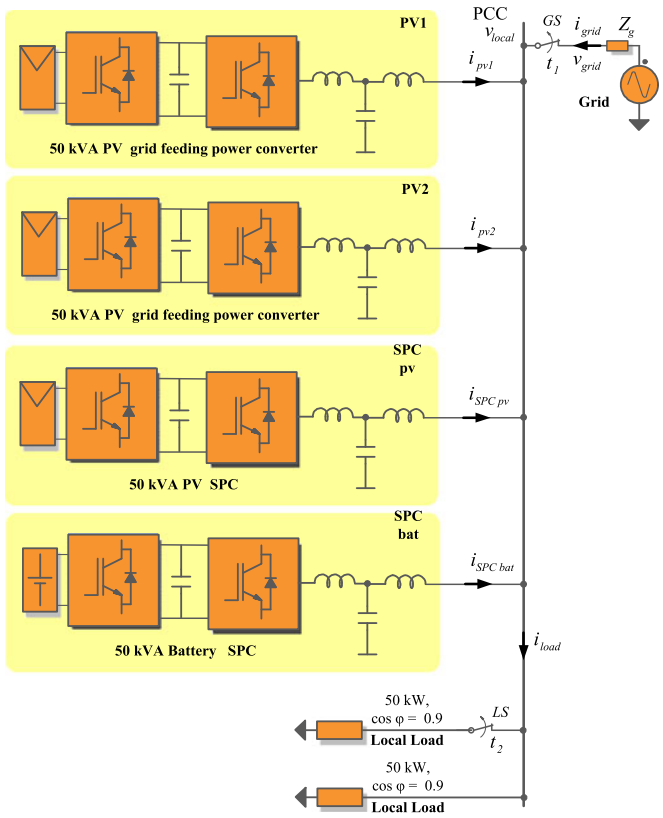

Fig. 5. Simulation study case consisting of: Two PV power plants controlled with grid-feeding converters PV_1 and PV_2, a PV plant and a battery controller through a SPC converter, SPCPV and SPCBAT, and two 50 kW inductive loads. The grid switch (GS) connects the system to the grid.

controller cannot be generically tuned. In this case, using the root-locus tool, the final placement of the poles can be seen in Fig. 4. As is proven from the location of the poles in the graph, the selected parameters give rise to a stable system with two dominant poles; hence, its response resembles the performance of a second-order system with the gain and phase margin values indicated previously.

IV. SIMULATION RESULTS

The structure of the simulation model implemented in this paper consists of four grids connected to 50 kVA power converters and two loads, as presented in Fig. 5. As can be seen in the figure, two of these converters belong to two PV power plants, PV_1 and PV_2, controlled in grid-feeding mode.

The other two will be SPC-controlled systems; a PV-based source will feed one of the SPC inverters, SPC_{PV}, and a grid-connected ES system will feed the last other one, SPC_{BAT}. In this study case, the load in the network consists of two elements, each absorbing 50 kW with a $\cos\Phi = 0.9$.

Table II shows the most important parameters of the SPC-based converters, while Table III gathers the data related to the grid-feeding PV converters. The virtual admittance is selected to be 3 in p.u., in order to match with the typical value of the transient admittance of synchronous generators. The real part of this admittance is 10 p.u., so that the transient and the possi-

TABLE II
SPC CONVERTER TECHNICAL DATA (2 CONVERTERS)

Symbol	Quantity	Value
S_{SPC}	nominal power	50 kVA
V_{DC}	nominal dc voltage	685 V
V_{AC}	nominal ac voltage	400 V
f_{AC}	nominal ac frequency	50 Hz
f_S	switching frequency	10 kHz
L	output filter inductors	0.68 mH
C	output filter capacitors	33 μF
k_P	active power drop ΔP/Δf	100 p.u.
k_Q	reactive power drop ΔQ/ΔV	10 p.u.
H	inertia constant	10 s

TABLE III
PV GRID-FEEDING TECHNICAL DATA (2 CONVERTERS)

Symbol	Quantity	Value
S	nominal power	50 kVA
V_{PV}	nominal dc voltage	685 V
V_{AC}	nominal ac voltage	400 V
f_{AC}	nominal ac frequency	50 Hz
$\cos\varphi$	power factor adjustment	1

TABLE IV
NETWORK AND LOAD PARAMETERS

Symbol	Quantity	Value
Scc_{grid}	short circuit power	2 MVA
P_{load}	nominal load active power	50 kW
Q_{load}	nominal load reactive power	24.2 kvar

TABLE V
SPC PARAMETERS

Symbol	QUANTITY	Value
R_V	virtual resistance	1.6 Ω
L_V	virtual inductance	15.3 mH
H	virtual inertia constant	5
ζ	damping ratio	1

ble resonances are attenuated quickly, resulting in a first-order time constant of 10 ms. In order to complete the information, Table IV summarizes the network and load parameters.

A. Steady-State Grid Connected Conditions

Initially, all the elements involved in the simulation are enabled and grid connected.

The converters of the plants PV_1 and PV_2 are controlled as grid-feeding converters, delivering 30 and 20 kW, respectively, at the beginning of the simulation. Both converters are equipped with active anti-islanding algorithm based on sensing the voltage and frequency deviations.

In these conditions, the SPC-controlled PV system provides also 30 kW, and, finally, the last converter, also equipped with SPC, is delivering zero current, as the battery is controlled for

TABLE VI
SPC-BASED POWER CONVERTER TECHNICAL DATA

Symbol	Quantity	Value
S_{SPC}	nominal power	10 kVA
V_{DC}	nominal dc voltage	685 V
V_{AC}	nominal ac voltage	400 V
f_{AC}	nominal ac frequency	50 Hz
f_S	switching frequency	10 kHz
C_{BUS}	dc bus capacitance	2.2 mF
L	output filter inductors	3.4 mH
C	output filter capacitors	4.7 μF

TABLE VII
AC TRANSFORMER TECHNICAL DATA

Symbol	Quantity	Value
S_T	nominal power	20 kVA
V_P	primary voltage	400 V
V_S	secondary voltage	400 V
f_T	nominal frequency	50–60 Hz
	connection type	YNyn0
η_{T}	efficiency	98%

TABLE VIII
COMMERCIAL CONVERTER TECHNICAL DATA (1 CONVERTER)

Symbol	Quantity	Value
S	nominal power	5 kVA
V_{PV}	dc voltage range	(150, 1000) V
V_{AC}	nominal ac voltage	400 V
f_{AC}	nominal ac frequency	50 Hz
$\cos\varphi$	adjustable power factor	[0.8, 1] over/under-excited

maintaining the energy balance of the system, especially when operating in island conditions.

B. Seamless Transition From Grid Connected to Island Mode Operation

After operating in the previous grid-connected steady state conditions, a fault in the main grid is generated in the simulation at $t = 0.8$ s, which produces a trip of the grid switch (GS), as shown in Fig. 5, thus leaving all the PV plants, the ESS, and the loads islanded.

The results in Fig. 6 show the behavior of the voltage and the currents in the different elements during the transient. As it can be seen in Fig. 6 at $t = 0.8$, when the system goes to island operation the resulting microgrid should adjust generation with consumption to remain in stable operation mode. PV_1 and PV_2 do not change their operation point, as they work with the standard MPPT grid-feeding control of PV inverters under the supervision of the anti-islanding algorithm, and they remain connected thanks to the fact that both SPC converters take care of forming the grid.

As proven by the obtained results, the voltage in the isolated system, v_{local}, as well as the current required for feeding the load, i_{load}, does not experience any transient that may affect their

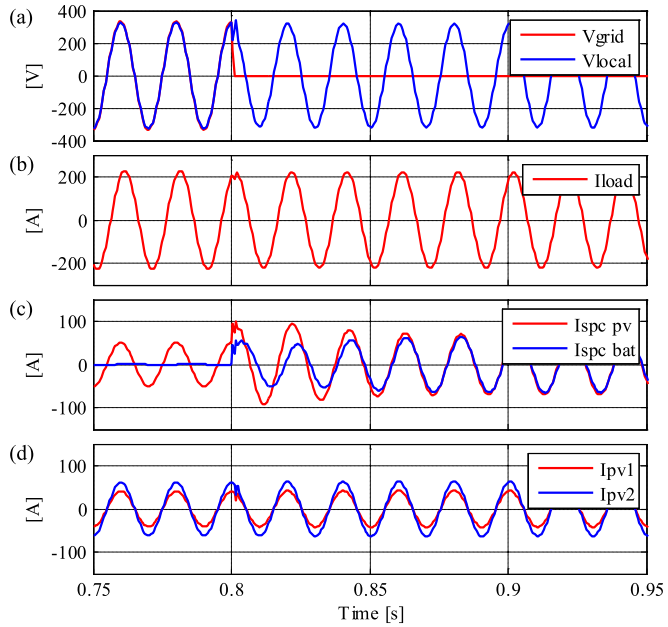

Fig. 6. Performance of the simulated system when there is an outage at $t = 0.8$ s. (a) Grid voltage and voltage at the PCC. (b) Current absorbed by the load. (c) Current injected by the SPCPV and the SPCBAT. (d) Current delivered by the PV_1 and PV_2 plants.

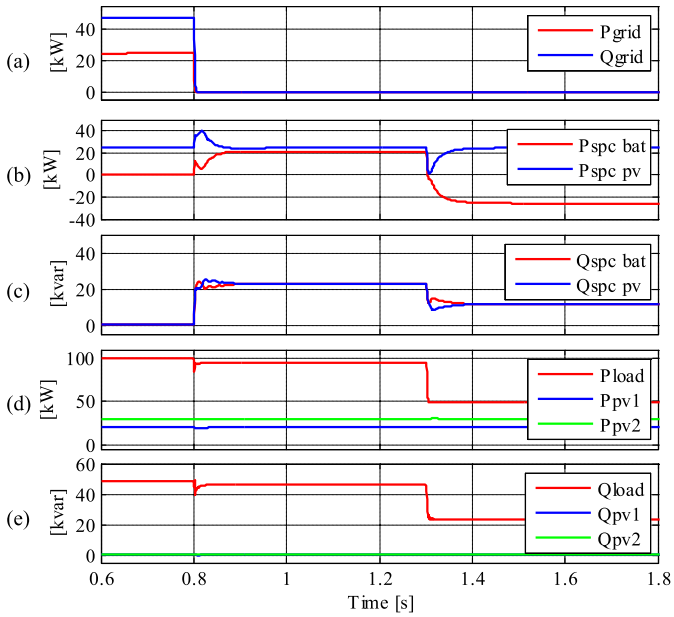

Fig. 7. Power delivery profile considering the network outage at $t = 0.8$ s and the 50 kW load disconnection at $t = 1.3$ s in island mode. (a) Active and reactive power delivered by the grid. (b) Active power delivered by the SPCPV and the SPCBAT. (c) Reactive power delivered by the SPCPV and the SPCBAT. (d) Active power consumed by the load and delivered by PV_1 and the PV_2. (e) Reactive power consumed by the load and delivered by PV_1 and the PV_2.

normal operation between grid-connected and island mode; this is due the action of the SPC power converters. This is even more noticeable in the case of the PV converters, as the two conventional plants and the one controlled with SPC remain operative without disconnecting, avoiding the trip that the anti-islanding would generate.

This performance evidences the instantaneous and smooth grid-forming capability of the SPC, proven by the fact that the anti-islanding algorithms were unable to detect the island.

As indicated previously, all these elements were initially grid connected, so the grid was handling the power balance. However, after the disconnection from the grid, there is an imbalance between the power generated and consumed in this test grid. Due to this, the SPC converter belonging to the SPC_{BAT} adapts the power delivery supplying the required active and reactive power for keeping the voltage and the frequency of the system, as can be noted in Fig. 7(a) and (b). The change in the power delivery coming from SPC_{BAT} can be understood from the variation of the injected current in Fig. 6(c).

Moreover, due to the inertia emulation, the SPC_{PV} also experiences a transient increase of the power delivered to the grid, in order to support the network frequency. This effect is due to the inertia, which extracts the power from the dc bus of the inverter, hence the shape of the currents delivered by the SPC_{PV} return to their initial value after some milliseconds, as can be noticed in Fig. 6(c). In Fig. 7, it can be seen that, after the transient, the power of the SPC–PV returns to its previous value. As the PV and the ESS do not rely on the same available energy, the performances of both are different, as the SPC_{PV} is only able to provide transient variation in the active power, whereas the SPC_{BAT} is able to change the power delivery for a longer time according to the energy stored in the battery.

During the island, the reactive power required by the load is shared between the two SPC-based converters, which rely on the same *Q–V* droop coefficients, with influence on stationary response, and equivalent output impedance, with influence on transient response. On the contrary, the conventional plants, PV_1 and PV_2, remain injecting the power demanded by the MPPT algorithm, and also do not take any action for balancing the reactive power. With a voltage variation of –5 V and a frequency change of –0.7 rad/s, the system finally reaches the equilibrium between generation and load.

C. Change in the Load When Operating in Island

Once the system of Fig. 5 is working in island mode, a change in the value of the load, and, thus, in the overall energy consumption, has been generated by means of opening the load switch, at $t = 1.3$ s, disconnecting one load of 50 kW with a $\cos\Phi = 0.9$.

This change introduces a transient imbalance between power generated and consumed and permits testing the capability of the SPC converters to restore the balance conditions without giving rise to undesired transient that may conduct to the disconnection of the other PV plants, PV_1 and PV_2. The results of this test, at $t = 1.3$ s, are presented in Figs. 8 and 9.

As can be observed from the simulation results, as shown in Fig. 8(c), the battery-based SPC converter, takes care of reestablishing the equilibrium point, by means of absorbing the excess of generated power.

During this transient, the voltage profile, as well as the currents absorbed by the loads and delivered by the generation systems, do not suffer any undesired transient perturbation, just the change in the average value of the power. The evolution of

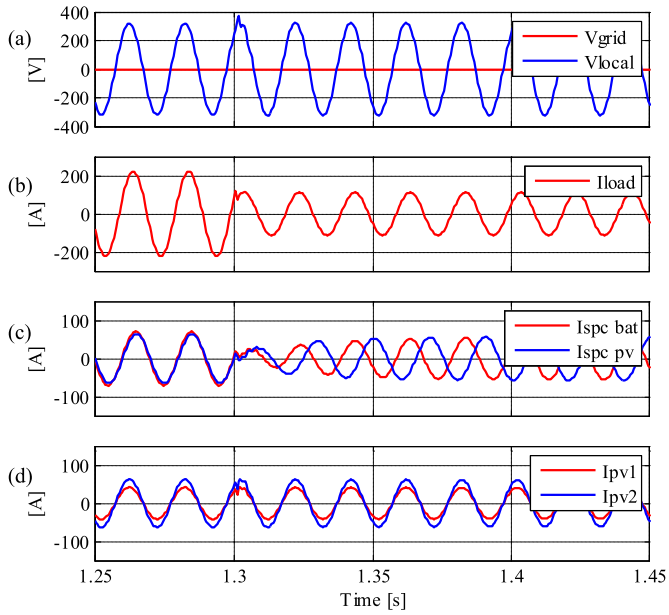

Fig. 8. Performance of the simulated system when there is a change in the load at $t = 1.3$ s. (a) Grid voltage and voltage at the PCC. (b) Current absorbed by the load. (c) Current injected by the $\mathrm{SPC_{PV}}$ and the $\mathrm{SPC_{BAT}}$. (d) Current delivered by the PV_1 and PV_2 plants.

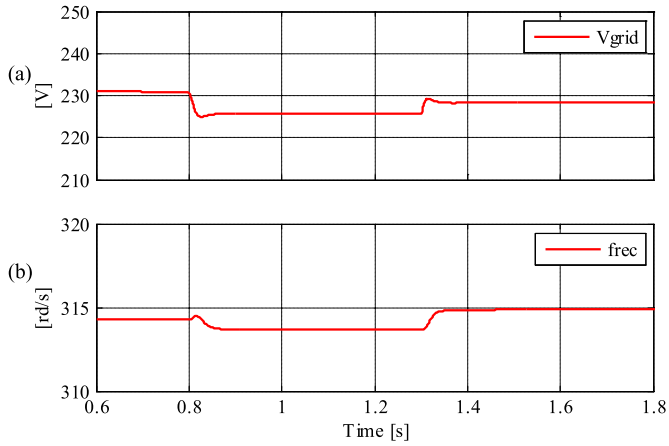

Fig. 9. Performance of the grid variables. (a) Phase to ground RMS value at the PCC. (b) Frequency at the PCC.

the voltage magnitude and frequency is shown in Fig. 9, where it can be stated that they remain within the admissible limits during the entire simulation, from grid connected to island mode including load changes.

This window resembles the one that the grid-feeding converters take into account for activating or not the anti-islanding trip, the *v–f* trajectory is presented in Fig. 10, where the boundaries are established considering the ENTSO-E directions. As in all conditions, the deviation in magnitude and frequency is so small, thanks to the SPC converter, that all the systems are able to operate under safe conditions.

V. Experimental Results

In the field of PV power converters, we have selected one of the most relevant manufacturers in terms of quality and market

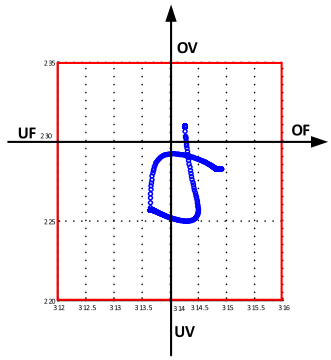

Fig. 10. Nondetection zone and transient evolution of *v* and *f*.

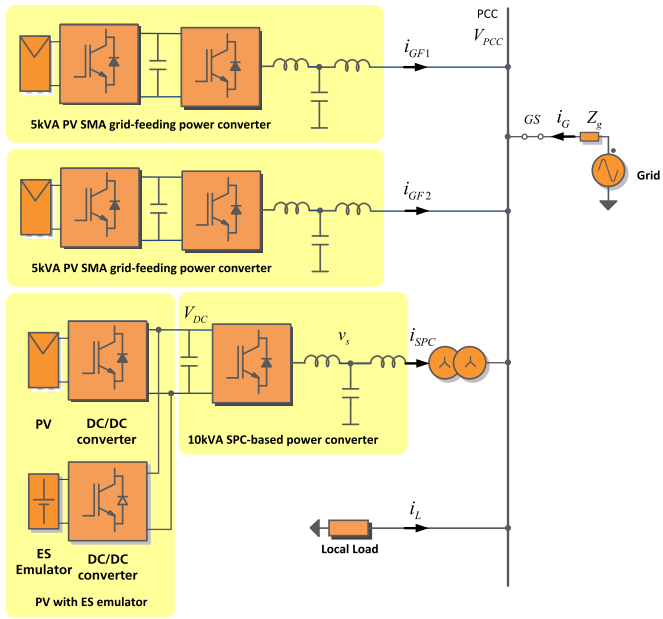

Fig. 11. Structure of the experimental test bench that consist of two 5-kW PV three-phase commercial converter connected to a PV small plant of six strings, one 10-kVA converter equipped with SPC controller connected to a PV string, a configurable load and a ES emulator connected to the dc bus of the SPC 10-kVA converter.

share. Therefore, the same system used in the simulation has been scaled down and assembled in the laboratory in order to test the performance of the SPC converter, using two 5 kVA commercial converters linked to a real PV plant and a customized SPC converter.

In the commercial inverters used, for the active islanding detection the set-point of the reactive current controller is continuously changed in order to allow inductive or capacitive power to be alternately fed into the grid. If the reactive power cannot be regulated, it means the grid is absent, so the inverter gets disconnected [33].

A. Specifications of the Study Case

The layout of the experimental platform used in this paper is depicted in Fig. 11, the same as the one presented in [34].

As can be clearly seen, at the PCC, the main ac system is connected to a local microgrid consisting of four parallelized

Fig. 12. Experimental setup implemented in the laboratory.

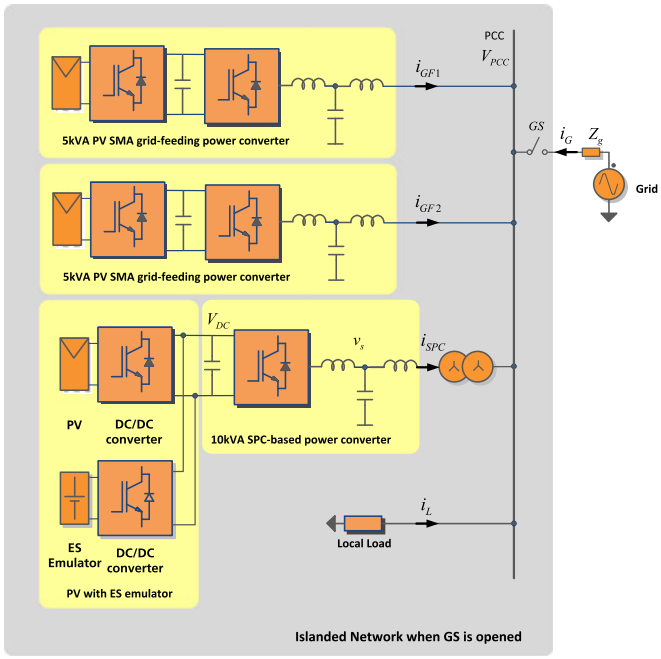

Fig. 13. Islanded network generated when the GS is opened. Elements: Two conventional PV converters, an SPC-equipped converter with PV, and ESS at the dc bus and a local load.

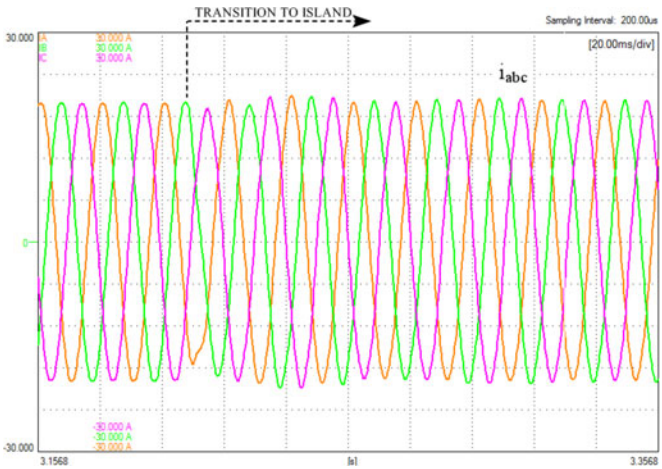

Fig. 14. Three-phase currents (i_L) absorbed by the load (6 A/div; 20 ms/div).

elements. From top to bottom in the figure, these elements are: two independent PV strings, each one feeding a commercial inverter; a power conversion prototype, in which two parallel dc–dc converters interfacing a PV plant and a battery bank, respectively, are linked through a common dc bus with a SPC-based inverter, in turn connected to the PCC by an *LC* filter and an isolating transformer, giving rise to an equivalent *LCL* connection, and, finally, a resistive load.

The control loops implementation of the SPC-based inverter prototype has been programmed in a dSpace 1103 commercial platform, which is also used for recording the results of the experiments. An actual picture of the assembled experimental setup is shown in Fig. 12.

All the technical parameters of the system are reported in Tables V–VIII.

B. Seamless Transition From Grid Connected to Island Mode

The possibility of forming an isolated grid is an intrinsic property of a synchronous generator. The experiment presented in this section aims indeed at testing the synchronous performances of an SPC-based switching power converter.

The microgrid illustrated in Fig. 11 has been set up and the steady-state conditions have been reached. With the resistive load absorbing about 10 kW and the PV panels producing about 4 kW, the main ac grid has been suddenly disconnected from the rest of the system. The disconnection from the main grid is performed by means of opening the grid with GS, giving rise to the isolated network presented in the Fig. 13.

In a conventional situation, the anti-islanding algorithm of the commercial converters would detect the disconnection of the mains and immediately cease the injection of currents. Nonetheless, the capability of the SPC-based inverter to act as a grid-forming element during and after the mains disconnection makes the anti-islanding system of the commercial inverters not able to detect the occurred transition and continues the PV power production without interruption. The recorded waveforms of the three-phase currents absorbed by the load, the PV inverters, and the grid are shown in Figs. 14–16, respectively. As visible from the figures, a small perturbation in both the load and PV currents is registered due to the transition to island mode. After the disconnection of the main grid, the SPC-based converter starts working automatically as a grid-forming element. In order to compensate the difference between the power produced by the PV panels and the one demanded by the three-phase resistive load, it automatically increases the amount of injected currents, as can be seen in Fig. 17. It should be noted that the magnetizing currents absorbed by the isolating transformer give rise to slight distortions in the measurements.

The main objective of the SPC is to keep stable, as much as possible, the three-phase voltage at the PCC, thus allowing the whole microgrid to carry on operating with no interruption.

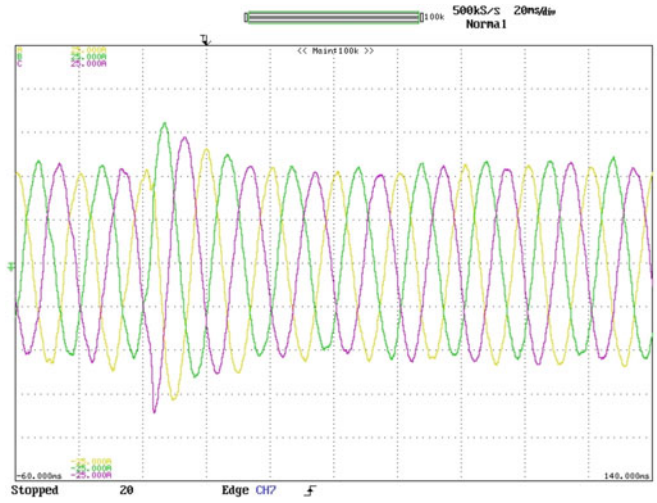

Fig. 15. Three-phase currents $(i_{GF1} + i_{GF2})$ at the output of the PV converters (3 A/div; 20 ms/div).

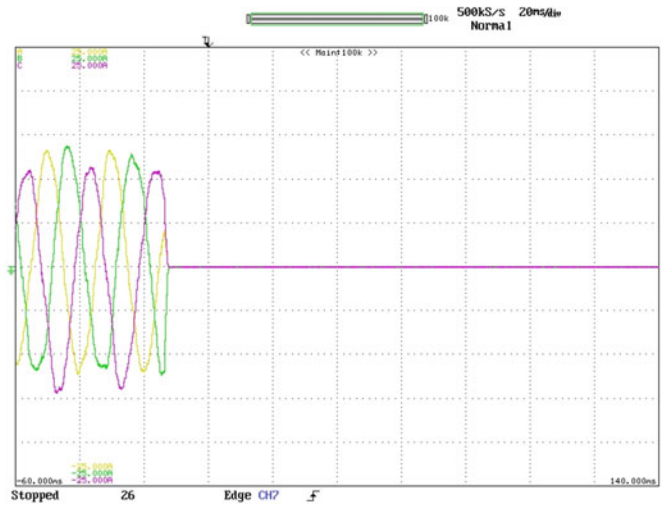

Fig. 16. Three-phase currents (i_G) provided by the network before and after the GS activation (3 A/div; 20 ms/div).

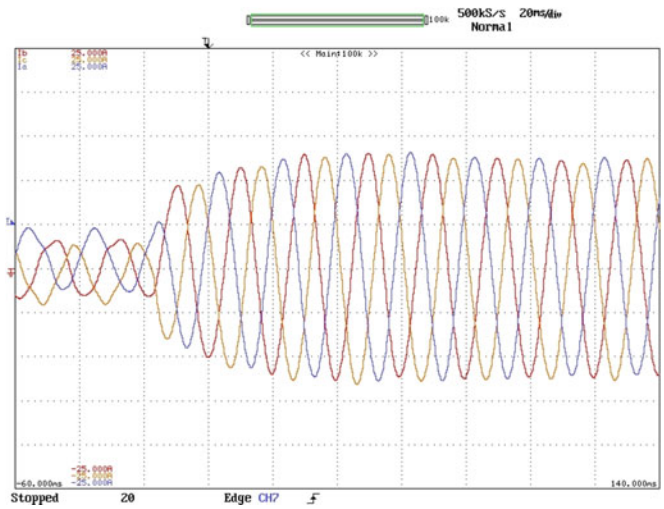

Fig. 17. Three-phase currents (i_{SPC}) provided by the SPC-based converter (5 A/div; 20 ms/div).

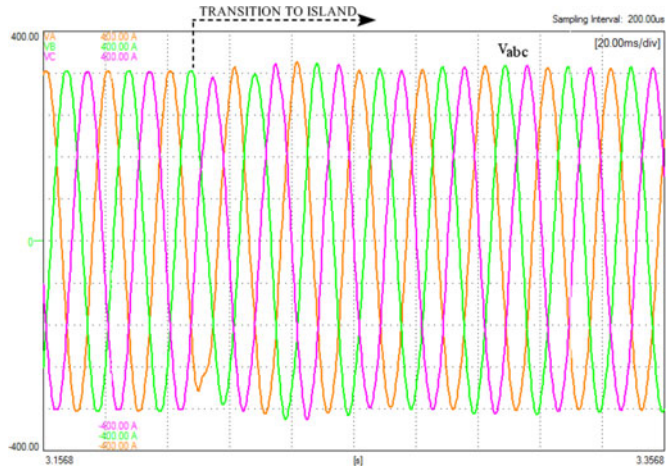

Fig. 18. Three-phase voltages profile at the PCC (80 V/div; 20 ms/div).

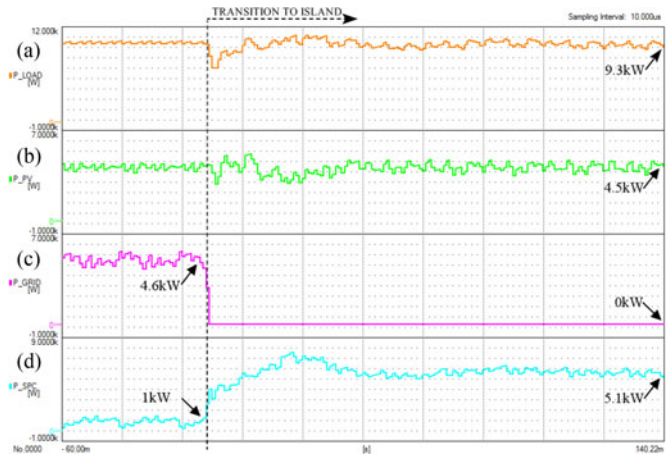

Fig. 19. (a) Instantaneous active power absorbed by the load. (b) Instantaneous active power delivered by the PV inverters. (c) Instantaneous active power delivered by the grid. (d) Instantaneous active power delivered by the SPC-based converter.

As shown in Fig. 18, except for the small perturbation registered during the transition to island mode, the quality of three-phase voltages generated by the SPC-based converter is comparable with that provided by the main ac system prior to the transition. The profile of active power generated/absorbed by the different elements connected to the microgrid during the experiment is finally shown in Fig. 19.

The results obtained with the SPC-based converter prove its high capability for acting as a grid-forming element during a transition from grid-connected to island mode. The good performance of the system keeps the voltage at the PCC within the limits specified by regulations, thus does not require the intervention of anti-islanding algorithm present in modern commercial PV inverters.

C. Seamless Synchronization and Reconnection to the Main Grid

The experiment presented in this section aims at testing the performances of an SPC-based switching power converter to

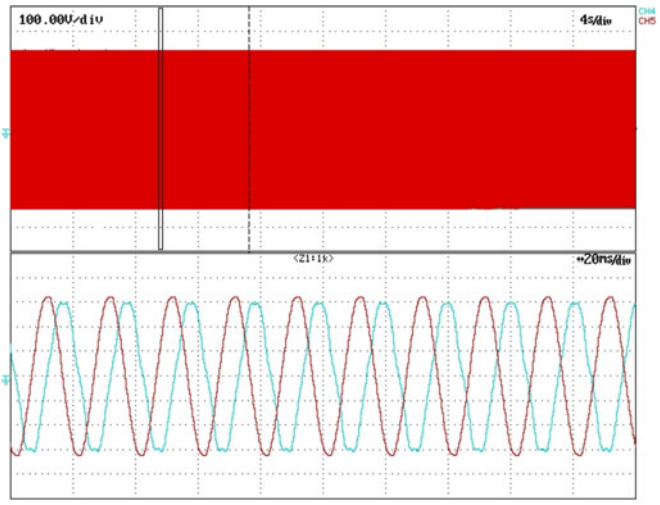

Fig. 20. Microgrid voltage and main ac grid voltage in one of the phases at the beginning of the process of synchronization (100 V/div; 4 s/div).

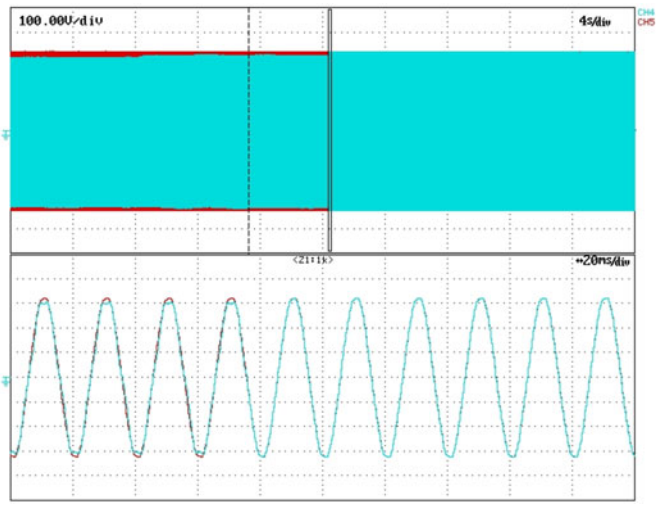

Fig. 21. Microgrid voltage and main ac grid voltage in one of the phases at the end of the process of synchronization (100 V/div; 4 s/div).

resynchronize the microgrid of Fig. 11 with the main ac system and allow a safe and smooth transition from intentional island mode to grid-connected mode.

In order to carry out this task, the SPC performs a process of grid-synchronization that brings the microgrid under the same conditions of the main ac grid in terms of voltages (same amplitude, same frequency, and same phase). During the whole process of synchronization, the anti-islanding system of the commercial inverters must not detect the island condition, thus ensuring the continuity of the PV power production.

The resynchronization can be performed following a slow profile, as the priority in the reconnection is to avoid the appearance of overcurrents/overvoltages that could give rise to a protection trip. In this paper, the resynchronization followed is the one proposed and described in detail in [35]. Taking advantage of the SPC capability to change the frequency in the microgrid, this value is changed slightly, in such a way that the frequency difference between the grid, while the microgrid is still in island mode, and the microgrid makes the phase difference between both changes smoothly. The phase difference between both is monitored by the control system of the microgrid, which is embedded in the SPC control board, and when it is crossing zero the GS is enabled and the microgrid gets connected to the main grid. The magnitude of the voltage is easier to track, as the measurement of this parameter in the grid is provided as a reference to the microgrid, which adapts the peak value to match the one in the grid. This process requires having two voltage measurement points, one at the grid side and another one at the microgrid side. However, these measurements are already necessary if such a system, able to work grid connected and islanded, is conceived.

After operating the microgrid of Fig. 11 in island mode, with the resistive load absorbing about 10 kW and the PV panels producing about 6 kW, the process of synchronization has been manually started. Figs. 20 and 21 show the microgrid voltage and the main ac grid voltage measured in one of the phases at the beginning and at the end of the synchronization.

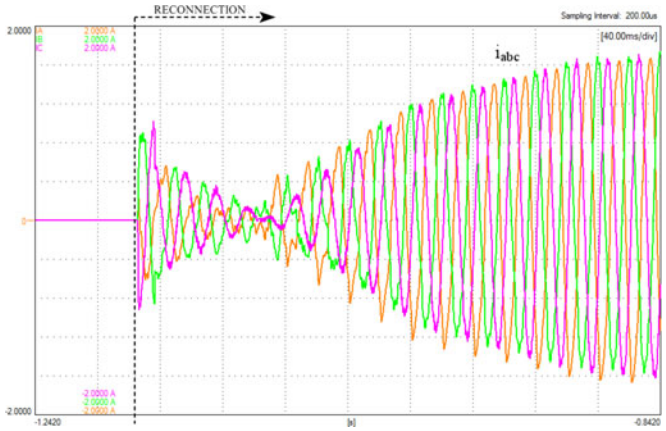

Fig. 22. Three-phase currents (i_G) supplied by the main ac grid (0.4 A/div; 40 ms/div).

Having achieved the synchronization, the external GS of Fig. 11 is closed, achieving the transition from island to grid-connected mode. The plots in Figs. 20 and 21 show the three-phase currents supplied by the main ac grid and the SPC-based converter during the reconnection.

Immediately after the reconnection, for a short instant, some of the power injected by the SPC-based converter is absorbed by the main ac grid, which offers a quite low impedance to the connected microgrid. Subsequently, after a slow transient determined essentially by the inertia constant fixed for the experiment (see H in Table IV), the output power of the SPC-based converter reaches its internal set point, which was manually fixed prior to the reconnection process at 3.3 kW.

During this phase, the behavior of the main ac grid changes, whereas, at the beginning, it absorbs some of the power injected by the SPC-based converter, at the end of the transient, it injects the necessary amount of power for compensating the difference between the one produced by the SPC-based converter and the one demanded by the load.

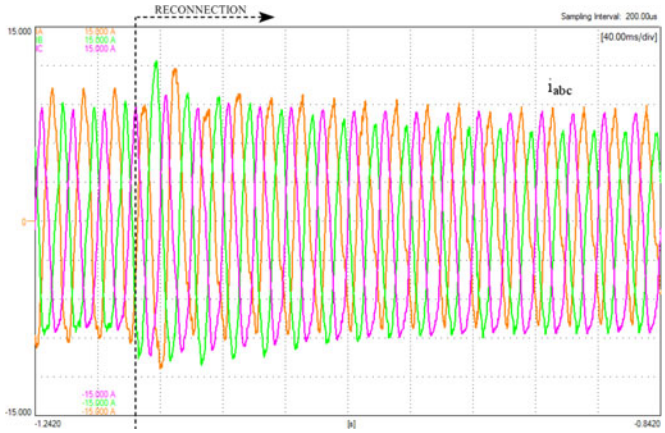

Fig. 23. Three-phase currents (i_{SPC}) provided by the SPC-based converter (3 A/div; 40 ms/div).

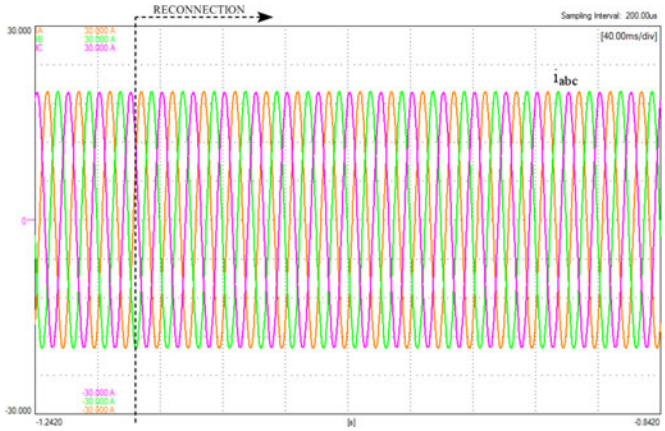

Fig. 24. Three-phase currents (i_L) absorbed by the load (6 A/div; 40 ms/div).

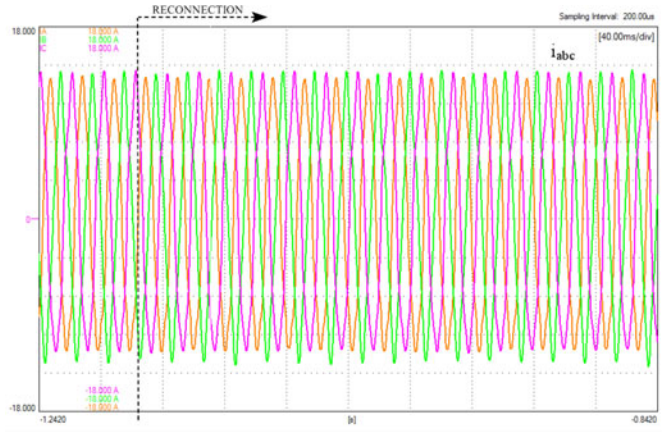

Fig. 25. Three-phase currents ($i_{\text{GF1}} + i_{\text{GF2}}$) produced by the PV inverters (3.6 A/div; 40 ms/div).

No perturbations are visible from the figures in correspondence of the microgrid reconnection to the main ac grid, thanks to the proper synchronization achieved between these two systems.

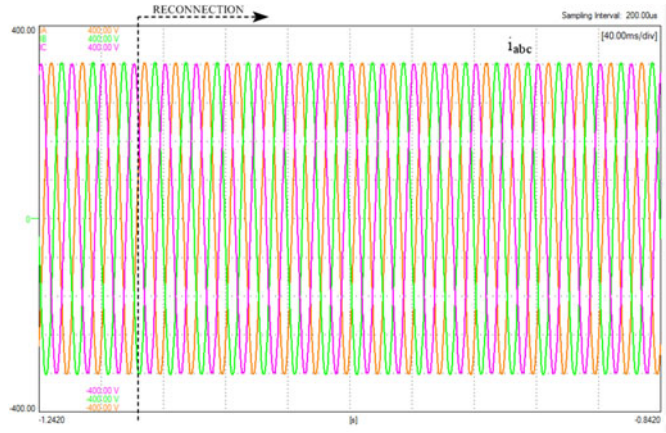

Fig. 26. Three-phase voltages profile at the PCC (80 V/div; 40 ms/div).

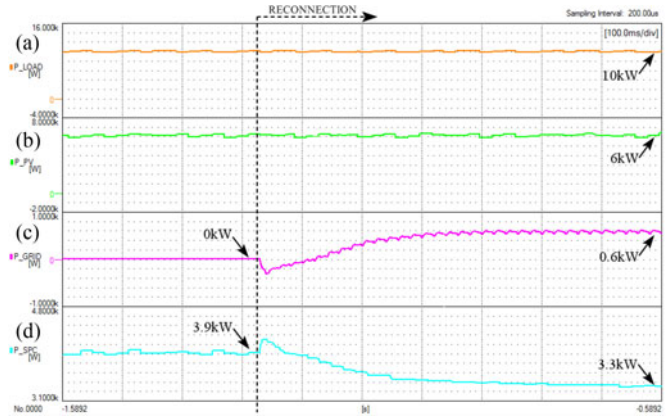

Fig. 27. (a) Instantaneous active power absorbed by the load. (b) Instantaneous active power delivered by the PV inverters. (c) Instantaneous active power delivered by the grid. (d) Instantaneous active power delivered by the SPC-based converter.

The reverse power flow at the PCC is visible also from Fig. 22, where the three-phase currents supplied by the grid exhibit a phase inversion some milliseconds after the reconnection.

Figs. 23–26 show the three-phase currents absorbed by the load, the three-phase currents produced by the PV panels, and the three-phase voltages profile at the PCC, respectively, during the reconnection transient.

The profile of active power generated/absorbed by the different elements involved during the experiment is finally shown in Fig. 27.

The obtained results prove the capability of the SPC-based converter to act as a grid-forming element and perform a perfect process of synchronization, allowing a safe transition of the microgrid from intentional island to grid-connected mode.

VI. Conclusion

In this paper, the advantages that the SPC controller introduces in the control of grid-connected power converter, its capability to create an isolated network, as well as in the

performance of other elements connected to the network, have been demonstrated.

As has been shown, the implementation of the SPC is simple and it can be integrated in a conventional power converter, keeping their inner controller and just adding the additional electrical and electromechanical characteristics.

The advantages of the proposed solution have been particularized for PV applications. In the simulation and experiments performed in this paper, it has been stated that an SPC-based PV power converter is able to operate seamlessly in grid-connected and island mode, something that will be required in the near future.

As has been shown, the correct performance of the system is even able to elude the anti-islanding algorithm of the connected commercial PV inverters, something that evidences the soft transitions and lack of undesired transients between grid and islanded operation modes. Moreover, it is able to prevent the trip of other generation systems, which are programmed to disconnect when the main grid experiences an outage, such as grid-feeding power PV power converters, and leave them safely operative in feeding the isolated network. In this case, it has been also shown how an ESS controlled with SPC is able to regulate the power balance between generation and demand.

The simulation analysis has permitted to validate the good performance when SPC converters are integrated in small-scale power plants. Likewise, the 30-kW test-bench have confirmed that no undesired transients appear, even avoiding the anti-islanding protection of a commercial PV converter.

Hence, the proposed approach has shown, in simulation and in an experimental setup, how the SPC is a useful control technique that permits to work a renewable-based generation system or ES system in grid-connected or islanded mode with such a soft-transition that even converters prepared and certified to detect the island conditions are unable to distinguish.

REFERENCES

[1] T. Mai *et al.*, "Renewable electricity futures for the united states," *IEEE Trans. Sustain. Energy*, vol. 5, no. 2, pp. 372–378, Apr. 2014.

[2] European Commission, "Renewable energy progress and biofuels sustainability," Mar. 2013. [Online]. Available: http://ec.europa.eu/energy/renewables/reports/doc/2013_renewable_energy_progress.pdf

[3] K. H. LaCommare and J. H. Eto, "Understanding the cost of power interruptions to U.S. electricity consumers," Environ. Energy Technol. Div., Univ. California Berkeley, Berkeley, CA, USA. Sep. 2004. [Online]. Available: http://certs.lbl.gov/pdf/55718.pdf

[4] B.-I. Craciun, T. Kerekes, D. Sera, and R. Teodorescu, "Overview of recent grid codes for PV power integration," in *Proc. Int. Conf. Optim. Elect. Electron. Equip.*, 2012, pp. 959–965.

[5] M. Tedde and K. Smedley, "Anti-islanding for three-phase one-cycle control grid tied inverter," *IEEE Trans. Power Electron.*, vol. 29, no. 7, pp. 3330–3345, Jul. 2014.

[6] Z. Ye, M. Dame, and B. Kroposki, "Grid-connected inverter anti-islanding test results for general electric inverter-based interconnection technology," Nat. Renewable Energy Lab., Golden, CO, USA, Tech. Rep. NREL/TP-560-37200, Jan. 2005. [Online] Available: http://www.nrel.gov/docs/fy05osti/37200.pdf

[7] D. Velasco, C. L. Trujillo, G. Garcerá, and E. Figueres, "Review of anti-islanding techniques in distributed generators," *Renew. Sustain. Energy Rev.*, vol. 14, no. 6, pp. 1608–1614, Aug. 2010.

[8] F. De Mango, M. Liserre, A. D. Aquila, and A. Pigazo, "Overview of anti-islanding algorithms for PV systems. Part I: Passive methods," in *Proc. 12th Power Electron. Motion Control Conf.*, 2006, pp. 1878–1883.

[9] S.-H. Lee and J.-W. Park, "New islanding detection method for inverter-based distributed generation considering its switching frequency," *IEEE Trans. Ind. Appl.*, vol. 46, no. 5, pp. 2089–2098, Sep./Oct. 2010.

[10] G. Hernandez-Gonzalez and R. Iravani, "Current injection for active islanding detection of electronically-interfaced distributed resources," *IEEE Trans. Power Del.*, vol. 21, no. 3, pp. 1698–1705, Jul. 2006.

[11] E. J. Estebanez, V. M. Moreno, A. Pigazo, M. Liserre, and A. Dell'Aquila, "Performance evaluation of active islanding-detection algorithms in distributed-generation photovoltaic systems: Two inverters case," *IEEE Trans. Ind. Electron.*, vol. 58, no. 4, pp. 1185–1193, Apr. 2011.

[12] H. Karimi, A. Yazdani, and R. Iravani, "Negative-sequence current injection for fast islanding detection of a distributed resource unit," *IEEE Trans. Power Electron.*, vol. 23, no. 1, pp. 298–307, Jan. 2008.

[13] J. Rocabert, A. Luna, F. Blaabjerg, and P. Rodríguez, "Control of power converters in AC microgrids," *IEEE Trans. Power Electron.*, vol. 27, no. 11, pp. 4734–4749, Nov. 2012.

[14] Y. A.-R. I. Mohamed, H. H. Zeineldin, M. M. A Salama, and R. Seethapathy, "Seamless formation and robust control of distributed generation microgrids via direct voltage control and optimized dynamic power sharing," *IEEE Trans. Power Electron.*, vol. 27, no. 3, pp. 1283–1294, Mar. 2012.

[15] I. Serban and C. Marinescu, "Control strategy of three-phase battery energy storage systems for frequency support in microgrids and with uninterrupted supply of local loads," *IEEE Trans. Power Electron.*, vol. 29, no. 9, pp. 5010–5020, Sep. 2014

[16] J. He, Y. W. Li, J. M. Guerrero, F. Blaabjerg, and J. C. Vasquez, "An islanding microgrid power sharing approach using enhanced virtual impedance control scheme," *IEEE Trans. Power Electron.*, vol. 28, no. 11, pp. 5272–5282, Nov. 2013.

[17] P. Rodriguez, I. Candela, C. Citro, J. Rocabert, and A. Luna, "Control of grid-connected power converters based on a virtual admittance control loop," in *Proc. 15th Power Electron. Appl.*, 2013, pp. 1–10.

[18] P. Rodriguez, I. Candela, and A. Luna, "Control of PV generation systems using the synchronous power controller," in *Proc. Energy Convers. Congr. Expo.*, 2013, pp. 993–998.

[19] P. Rodriguez, J. I. Candela, J. Rocabert, and R. Teodorescu, "Virtual admittance controller based on static power converters," Int. Patent WO 2012/117133, Sep. 7, 2012.

[20] P. Rodriguez, J. I. Candela, J. Rocabert, and R. Teodorescu, "Controller of the virtual electromechanical characteristics for static power converters," Int. Patent WO 2012/117133, Sep. 7, 2012.

[21] P. Rodriguez, J. I. Candela, J. Rocabert, and R. Teodorescu, "Synchronous power controller of a generation system based on static power converters," Int. Patent WO 2012/117133, Sep. 7, 2012.

[22] Z. Lidong, L. Harnefors, and H. P. Nee, "Power-synchronization control of grid-connected voltage-source converters," *IEEE Trans. Power Syst.*, vol. 25, no. 2, pp. 809–820, May 2010.

[23] Q.-C. Zhong, N. Phi-Long, M. Zhenyu, and S. Wanxing, "Self-synchronized synchronverters: Inverters without a dedicated synchronization unit," *IEEE Trans. Power Electron.*, vol. 29, no. 2, pp. 617–630, Feb. 2014.

[24] Q.-C. Zhong and T. Hornik, *Control of Power Inverters in Renewable Energy and Smart Grid Integration*. Hoboken, NJ, USA: Wiley, 2013.

[25] H.-P. Beck, A. Dowrueng, J. Z. Hingst, M. A. J. M'buy, and E.–A. Wehrmann, "The clausthal demonstration plant for decentralised renewable energy supply systems - clausthal energy park -," in *Proc. Int. Conf. Clean Elect. Power*, 2007, pp. 41–44.

[26] K. De Brabandere, B. Bolsens, J. Van den Keybus, A. Woyte, J. Driesen, and R. Belmans, "A voltage and frequency droop control method for parallel inverters," *IEEE Trans. Power Electron.*, vol. 22, no. 4, pp. 1107–1115, Jul. 2007.

[27] K. De Brabandere, "Voltage and frequency droop control in low voltage grids by distributed generators with inverter front-end," Ph.D. dissertation, Elect. Eng. Dept., , Katholieke Universiteit Leuven, Leuven, België, 2006.

[28] J. Kim, J. Guerrero, P. Rodriguez, R. Teodorescu, and K. Nam, "Mode adaptive droop control with virtual output impedances for an inverter-based flexible AC microgrid," *IEEE Trans. Power Electron.*, vol. 26, no. 3, pp. 689–701, Mar. 2011.

[29] Q.-C. Zhong and G. Weiss, "Static synchronous generators for distributed generation and renewable energy," in *Proc. Power Syst. Conf. Expo.*, 2009, pp. 1–6.

[30] Q.-C. Zhong and G. Weiss "Synchronverters: inverters that mimic synchronous generators," *IEEE Trans. Ind. Electron.*, vol. 58, no. 4, pp. 1259–1267, Apr. 2011.

[31] L. Zhang, L. Harnefors, and H.-P. Nee, "Power-synchronization control of grid-connected voltage-source converters," *IEEE Trans. Power Syst.*, vol. 25, no. 2, pp. 809–820, May 2010.
[32] R. Teodorescu, M. Liserre, and P. Rodriguez, *Grid Converters for Photovoltaic and Wind Power Systems*, 1st ed. Hoboken, NJ, USA: Wiley, 2011.
[33] SMA, SMA Solar Technol., Niestetal, Germany, "Description of grid monitoring and active islanding detection," May 2016. [Online]. Available: www.ledico.com/_Uploads/dbsAttachedFiles/kovetz.pdf
[34] P. Rodriguez, C. Citro, I. Candela, J. Rocabet, and A. Luna, "Flexible grid connection and islanding of SPC-based PV power converters," in *Proc. IEEE Energy Convers. Congr. Expo*., Montreal, QC, Canada, 2015, pp. 450–459.
[35] J. Rocabert, G. M. S. Azevedo, A. Luna, J. M. Guerrero, J. I. Candela, and P. Rodríguez, "Intelligent connection agent for three-phase grid-connected microgrids," *IEEE Trans. Power Electron.*, vol. 26, no. 10, pp. 2993–3005, Oct. 2011.

Pedro Rodríguez (SM'10 –F'13) received the M.Sc. and Ph.D. degrees in electrical engineering from the Technical University of Catalonia (UPC), Barcelona, Spain, in 1991 and 2004, respectively.

In 1990, he joined the UPC, where he became the Director of the Research Center on Renewable Electrical Energy Systems and still collaborates with the UPC as a Visiting Professor. In 2005, he was a Visiting Researcher at the Center for Power Electronics Systems, Virginia Tech. In 2006 and 2007, he was a Postdoctoral Researcher in the Department of Energy Technology, Aalborg University (AAU). From 2007 to 2011, he was a co-supervisor of the Vestas Power Program with AAU. From 2011 to 2017, he was the Director of Technology in the area of power systems in Abengoa Research, Spain. Since 2017, he has been a Full Professor with Loyola University Andalucia, Seville, Spain. He has co-authored one Wiley/IEEE book, more than 80 papers in ISI technical journals, and around 250 papers in conference proceedings. He is the holder of 14 licensed patents. His research interests include distributed power systems, flexible transmission systems, and power conversion.

Dr. Rodriguez is an Associate Editor for the IEEE TRANSACTION ON POWER ELECTRONICS, and a member of the Sustainability and Renewable Energy Committee of the IEEE Industry Application Society and the Renewable Energy Systems Technical Committee of the Industrial Electronics Society.

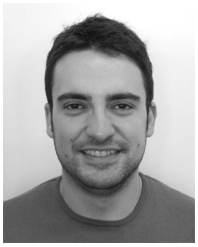

Costantino Citro received the M.Sc. degree in electronic engineering from the University of Salerno, Fisciano, Italy, in 2010.

He is with the Department of Industrial Engineering, University of Salerno. He has been working on multiple research and development projects in both industrial and academic settings, covering a wide range of disciplines such as power electronics, electrical power systems, digital signal processing, machine learning algorithms, and more recently, railway systems.

Joan Rocabert (S'08–M'11) received the M.Sc. and Ph.D. degrees in electrical engineering from the Technical University of Catalonia, Barcelona, Spain, in 2003 and 2010, respectively.

From 2004 to 2008, he was a Research Assistant in the Department of Electronic Engineering, Technical University of Catalonia, where since 2008, he has been a Researcher and an Assistant Professor with the Department of Electrical Engineering. His current research interests include power electronics, photovoltaics, wind energy systems, and microgrids.

J. Ignacio Candela (S'99–M'04) received the B.S. and M.S. degrees in industrial engineering and the Ph.D. degree in electrical engineering from the Technical University of Catalonia (UPC), Barcelona, Spain, in 1987, 2000, and 2009, respectively.

In 1990, he became an Assistant Professor with UPC, where he later advanced to Associate Professor in 1993 and is currently a part of the research group on Renewable Electrical Energy Systems, Department of Electrical Engineering. He has authored or co-authored more than 80 published technical papers, and holds several patents. His current research interests include power conditioning, integration of distributed energy systems, and control of grid connected power converters.

Alvaro Luna (S'07–M'10) received the B.Sc., M.Sc., and Ph.D. degrees from the Technical University of Catalonia (UPC), Barcelona, Spain, in 2001, 2005, and 2009, respectively, all in electrical engineering.

He was a Faculty Member with the UPC in 2005, where he is currently an Assistant Professor. His research interests include wind turbines control, photovoltaic systems, integration of distributed generation, and power conditioning.